Journal of Power Sources 217 (2012) 248–255

Contents lists available at SciVerse ScienceDirect

Journal of Power Sources

journal homepage: www.elsevier.com/locate/jpowsour

Lithium ion cell modeling using orthogonal collocation on finite elements

Long Cai, Ralph E. White*

Department of Chemical Engineering, University of South Carolina, Swearingen Engineering Center, 301 Main Street, Columbia, SC 29208, USA

HIGHLIGHTS

► The OCFE method was applied to efficiently solve the diffusion equation in a solid particle.
► The OCFE method was compared to some other methods for the diffusion equation in a solid particle.
► The OCFE method was used to solve the P2D model to reduce the computation time.

ARTICLE INFO

Article history:
Received 2 April 2012
Received in revised form
8 June 2012
Accepted 9 June 2012
Available online 19 June 2012

Keywords:
Lithium ion cell
Orthogonal collocation on finite elements
Modeling
Laplace transform

ABSTRACT

The physics-based pseudo two-dimensional (P2D) model for lithium ion cells requires significant computation time. To reduce this burden, the orthogonal collocation on finite elements (OCFE) method is applied here. The number of node points both in the macro-scale and in the micro-scale in the P2D model is reduced by optimally locating the node points. This OCFE method is shown to be better than other approximate methods for the spherical diffusion equation with flux boundary conditions. This OCFE method is also used to solve the P2D model equations and the results are compared to those obtained from COMSOL (a commercial differential/algebraic equation solver using FEM).

1. Introduction

A model with accurate short time response is important for the simulation of lithium ion cells in the applications with high rate charge/discharge processes. The pseudo two-dimensional (P2D) model developed by Doyle, Fuller, and Newman [1,2] has been widely used to simulate the performance of lithium ion cells with high rates. The P2D model is a physics-based model which includes material balances and charge balances in the solid phases and the electrolyte. The governing equations for the concentration of the electrolyte, the solid phase potential, and the electrolyte potential are solved in the macro-scale (the direction of the current passing through the cell). The governing equation for the concentration of lithium ions in the solid phase is established in the radial direction (the pseudo second dimension) in the active spherical particles. The macro-scale and the micro-scale (the solid particles) are coupled through the equation for the transfer of lithium ions from the electrolyte to the solid particles. Both the macro-scale and the micro-scale equations must be solved to obtain model predictions. Because of the multi-scale nature of the P2D model, significant computation time is required to solve the model equations using numerical methods [3,4]. To reduce this computation time, several approximation methods have been applied to simplify the diffusion equation in the solid phase. These methods include the polynomial approximation method [5], the residual grouping method [6], the diffusion length method [7], the mixed finite difference method [8], and the proper orthogonal decomposition (POD) based on the finite volume method (FVM) [3,4]. In this paper the orthogonal collocation on the finite elements (OCFE) method is used to reduce the computation time by reducing the number of node points in both the macro-scale and the micro-scale without sacrificing the accuracy of the predictions from the model. These methods are reviewed for spherical diffusion with flux boundary condition and compared to the OCFE method. After that the OCFE method is applied to the complete P2D model and the results are compared to those obtained from COMSOL.

2. Transient response for the surface concentration of lithium ions in a spherical particle

The governing equation of the concentration of lithium ions in a spherical particle is given by Fick's second law:

* Corresponding author. Tel.: +1 803 777 3270; fax: +1 803 777 0973.
E-mail address: white@cec.sc.edu (R.E. White).

0378-7753/$ – see front matter © 2012 Elsevier B.V. All rights reserved.
http://dx.doi.org/10.1016/j.jpowsour.2012.06.043

$$\frac{\partial c_s}{\partial t} = \frac{D_s}{r^2}\frac{\partial}{\partial r}\left(r^2\frac{\partial c_s}{\partial r}\right) \quad (1)$$

where D_s is the diffusion coefficient of lithium ions in the particle. At the center of the particle, there is no molar flux:

$$-D_s\frac{\partial c_s}{\partial r}\bigg|_{r=0} = 0 \quad (2)$$

The molar flux at the surface of the particle equals the reaction rate:

$$-D_s\frac{\partial c_s}{\partial r}\bigg|_{r=R_s} = \frac{j(t)}{a_s F} \quad (3)$$

where R_s is the radius of the particle; $j(t)$ denotes the current density of the lithium insertion/deintercalation reaction; a_s is the specific area; and F is Faraday's constant. Initially, it is assumed that the concentration of lithium ions is uniformly distributed in the particle:

$$c_s(r,0) = c_{s,0} \quad (4)$$

First, define a new variable, $\bar{c}_s(r,t) = c_s(r,t) - c_{s,0}$, where the initial concentration is subtracted from the concentration in the solid particles. The model equations for $\bar{c}_s$ are similar to those for c_s except that the initial condition for $\bar{c}_s$ is zero, and are presented as follows:

$$\frac{\partial \bar{c}_s}{\partial t} = \frac{D_s}{r^2}\frac{\partial}{\partial r}\left(r^2\frac{\partial \bar{c}_s}{\partial r}\right) \quad (5)$$

$$-D_s\frac{\partial \bar{c}_s}{\partial r}\bigg|_{r=0} = 0 \quad (6)$$

$$-D_s\frac{\partial \bar{c}_s}{\partial r}\bigg|_{r=R_s} = \frac{j(t)}{a_s F} \quad (7)$$

$$\bar{c}_s(r,0) = 0 \quad (8)$$

For comparison purpose, the transfer function, $g(r,s)$, of $\bar{c}_s(r,t)$ with respect to the input $j(t)$ can be obtained by using the Laplace transform method as follows [9]:

$$g(r,s) = \frac{\bar{c}_s(r,s)}{j(s)} = \frac{R_s^2}{a_s D_s F r}\frac{\sinh\left(r\sqrt{s/D_s}\right)}{\sinh\left(R_s\sqrt{s/D_s}\right) - R_s\sqrt{s/D_s}\cosh\left(R_s\sqrt{s/D_s}\right)} \quad (9)$$

where s is the independent variable in the Laplace domain. The analytical transfer function evaluated on the particle surface is given by:

$$g(R_s,s) = \frac{\bar{c}_s(R_s,s)}{j(s)} = \frac{R_s}{a_s D_s F}\frac{\tanh\left(R_s\sqrt{s/D_s}\right)}{\tanh\left(R_s\sqrt{s/D_s}\right) - R_s\sqrt{s/D_s}} \quad (10)$$

Next, define the averaged value of $\bar{c}_s(r,t)$ in the particle as:

$$\bar{c}_{s,avg}(t) = \frac{3}{R_s^3}\int_0^{R_s} r^2\bar{c}_s(r,t)dr \quad (11)$$

The transfer function for the averaged concentration can be obtained by substituting Eq. (9) into Eq. (11), that is:

$$\frac{\bar{c}_{s,avg}(s)}{j(s)} = -\frac{3}{R_s a_s F s} \quad (12)$$

The difference between the surface concentration and the averaged concentration can be defined as follows:

$$\Delta c_{s,R_s}(t) = \bar{c}_s(R_s,t) - \bar{c}_{s,avg}(t) \quad (13)$$

The transfer function for Eq. (13) is given by:

$$\frac{\Delta c_{s,R_s}(s)}{j(s)} = \frac{\bar{c}_s(R_s,s)}{j(s)} - \frac{\bar{c}_{s,avg}(s)}{j(s)} \quad (14)$$

Note that Eq. (14) has a finite steady state. Some simplified models for spherical diffusion in the Laplace domain are reviewed next.

2.1. Two-term polynomial approximation

The two-term polynomial approximation [5] to Eqs. (5)–(8) is given by one ordinary differential equation and one algebraic equation:

$$\frac{d\bar{c}_{s,avg}(t)}{dt} = -\frac{3}{R_s a_s F}j(t) \quad (15)$$

$$\bar{c}_s(R_s,t) - \bar{c}_{s,avg}(t) = -\frac{R_s}{5D_s a_s F}j(t) \quad (16)$$

The transfer function for Eq. (16) is:

$$\frac{\bar{c}_s(R_s,s) - \bar{c}_{s,avg}(s)}{j(s)} = -\frac{R_s}{5D_s a_s F} \quad (17)$$

2.2. Three-term polynomial approximation

The three-term polynomial approximation [5] to Eqs. (5)–(8) is:

$$\frac{d\bar{c}_{s,avg}(t)}{dt} = -\frac{3}{R_s a_s F}j(t) \quad (18)$$

$$\frac{dq_{avg}(t)}{dt} = -\frac{30D_s}{R_s^2}q_{avg}(t) - \frac{45}{2R_s^2 a_s F}j(t) \quad (19)$$

$$\bar{c}_s(R_s,t) - \bar{c}_{s,avg}(t) = \frac{8}{35}R_s q_{avg}(t) - \frac{35R_s}{D_s a_s F}j(t) \quad (20)$$

where $q_{avg}(t)$ is the volume averaged flux and is defined in Ref. [5] with the initial condition: $q_{avg}(0) = 0$. The transfer function for Eq. (20) is:

$$\frac{\bar{c}_s(R_s,s) - \bar{c}_{s,avg}(s)}{j(s)} = -\frac{R_s\left(sR_s^2 + 210D_s\right)}{35D_s a_s F\left(sR_s^2 + 30D_s\right)} \quad (21)$$

2.3. Residues grouping [6]:

The analytical transfer function for the surface concentration difference ($\Delta c_{s,Rs}(t)$) shown in Eq. (14) can be expanded into poles, p_k, and the associated residues, res_k,. [6]. These poles and residues are sorted such that the values of the poles are in the descending order. The analytical transfer function shown in Eq. (14) can be approximated by a finite number of poles and their residues:

$$\frac{\Delta c_{s,R_s}(s)}{j(s)} \doteq Z + \sum_{k=1}^{N}\frac{s\cdot res_k}{s - p_k} \quad (22)$$

where Z is the steady state value of the analytical transfer function; p_k is the kth pole of the analytical transfer function; and res_k is the

residue associated with p_k. The expression for Z can be obtained analytically:

$$Z = -\frac{R_s}{5D_s a_s F} \tag{23}$$

The N poles and residues in Eq. (22) can be divided into groups (say m groups, where $m << N$). In this work, the range of the ten based logarithm for the absolute values of the N poles is uniformly partitioned into m segments. The corrected residue and pole for each segment are given by:

$$\text{res}_{g,i} = \sum_{k=k_{g,i-1}+1}^{k_{g,i}} \text{res}_k, \quad i = 1 \cdots m \tag{24}$$

$$p_{g,i} = \frac{\sum_{k=k_{g,i-1}+1}^{k_{g,i}} p_k \text{res}_k}{\text{res}_{g,i}} \tag{25}$$

where $k_{g,i}$, $i = 0,1,\ldots,m$ is the index for the bounds of the pole segments. Then, the approximation to Eq. (22) using the method of residue grouping using the analytical transfer function is given by:

$$\frac{\Delta c_{s,R_s}(s)}{j(s)} \doteq Z + \sum_{k=1}^{m} \frac{s \cdot \text{res}_{g,k}}{s - p_{g,k}} \tag{26}$$

2.4. Finite volume method [3]:

The geometry discretization for a particle using FVM is shown in Fig. 1. The 1D geometry is divided uniformly into n control volumes (CVs) with size of h. The node points are located at the center of the control volumes. Control volume "P" is represented by its node point "P" and has two faces: face "w" and face "e". The two neighbor points of "P" are the point "W" and the point "E". It is assumed that the concentrations in the control volumes are piecewise continuous, that is the concentration in control volume "P" is uniformly distributed and is equal to the concentration at node point "P". The discrete model using the FVM is obtained by integrating Eq. (5) in each control volume (see Ref. [3] for the details). The resulting discrete model in matrix notation is given by:

$$\dot{\underline{C}} = \mathrm{A}\underline{C}(t) + \underline{b}j(t) \tag{27}$$

where $\underline{C} = [\bar{c}_{s,1}, \bar{c}_{s,2}, \ldots, \bar{c}_{s,n}]^T$, superscript "T" means matrix transpose; the dot over C means time derivative. Matrix A in Eq. (27) is an $n \times n$ tridiagonal matrix and includes the diffusivity and the geometry information. The concentration on the particle surface shown by an open circle in Fig. 1 at $r = R_s$ is not solved directly in Eq. (27) but it can be obtained by applying the three-point backward difference approximation to the flux on the surface, after Eq. (27) has been solved:

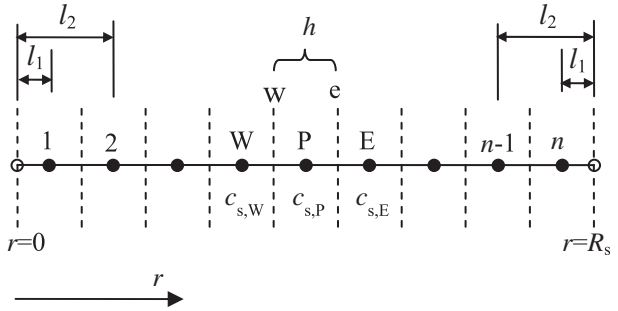

Fig. 1. Discretized geometry for the diffusion problem using the finite volume method ($l_1 = 0.5h$, $l_2 = 1.5h$).

$$\bar{c}_s(R_s,t) = \frac{9}{8}\bar{c}_{s,n}(t) - \frac{1}{8}\bar{c}_{s,n-1}(t) - \frac{3h}{8D_s a_s F} j(t) \tag{28}$$

The Laplace transform of Eq. (27) is given by:

$$\underline{G}(s) = \frac{\underline{C}(s)}{j(s)} = (\mathrm{I}s - \mathrm{A})^{-1}\underline{b} \tag{29}$$

where $\underline{G}(s)$ is a n by 1 vector and I is a n by n identity matrix. Based on Eqs. (12), (28) and (29), the transfer function of the surface concentration difference using the FVM is given by:

$$\frac{\Delta c_{s,R_s}(s)}{j(s)} = \frac{9}{8}G_n(s) - \frac{1}{8}G_{n-1}(s) - \frac{3h}{8D_s a_s F} + \frac{3}{R_s a_s F s} \tag{30}$$

where $G_{n-1}(s)$ and $G_n(s)$ are the $(n\text{-}1)^{\text{th}}$ and the nth element of $G(s)$ in Eq. (29).

2.5. Residue grouping using the state space approach [6]:

The transfer function shown in Eq. (29) has a zero pole ($s = 0$). To get rid of this pole at the origin, the first equation was subtracted from Eq. (2) through n shown in Eq. (27). The resulting equations are given by:

$$\dot{\underline{\chi}} = \widehat{\mathrm{A}}\underline{\chi}(t) + \underline{\hat{b}}j(t) \tag{31}$$

where $\chi_i = \bar{c}_{s,i+1} - \bar{c}_{s,1}$, $i = 1,\ldots,n-1$; $\widehat{\mathrm{A}}$ is an n-1 by n-1 matrix with $\widehat{\mathrm{A}}_{i,j} = \mathrm{A}_{i+1,j+1} - \mathrm{A}_{1,j+1}$, $i,j = 1,\ldots,n-1$; and $\underline{\hat{b}}$ is an n-1 by 1 vector with $\hat{b}_i = \underline{b}_{i+1} - \underline{b}_1$, $i = 1,\ldots,n-1$. Next define the output as:

$$\underline{y}(t) = \mathrm{C}\underline{\chi}(t) \tag{32}$$

where C is an n-1 by n-1 identity matrix. The transfer function for this state space approach is given by:

$$\frac{\underline{y}(s)}{j(s)} = \underline{Z} + \sum_{k=1}^{n-1} \frac{\underline{r}_k s}{s - \lambda_k} \tag{33}$$

where:

$$\underline{Z} = -\mathrm{C}\widehat{\mathrm{A}}^{-1}\underline{\hat{b}} \tag{34}$$

$$\underline{r}_k = \frac{\mathrm{C}\underline{q}_k \underline{p}_k \underline{\hat{b}}}{\lambda_k}, \quad k = 1,2,\ldots,n-1 \tag{35}$$

$\underline{q}_k$ is the kth eigenvector associated with the kth eigenvalue λ_k in the expansion of $\widehat{\mathrm{A}}$:

$$\widehat{\mathrm{A}}\mathrm{Q} = \mathrm{Q}\Lambda \tag{36}$$

$\underline{q}_k$ is the kth column in Q; Λ is a diagonal matrix and its non-zero elements are the eigenvalues of matrix $\widehat{\mathrm{A}}$. The vector $\underline{p}_k$ is the kth row in matrix P where $\mathrm{P} = \mathrm{Q}^{-1}$. In the modal form, the matrices $\widehat{\mathrm{A}}$, $\underline{\hat{b}}$, and C in Eqs. (31) and (32) are equivalent to :

$$\mathrm{A}^* = \mathrm{diag}(\lambda_1, \lambda_2, \ldots, \lambda_{n-1}) = \Lambda \tag{37}$$

$$\overset{*}{\underline{b}} = [1, 1, \ldots, 1]^T \tag{38}$$

$$\mathrm{C}^* = [\lambda_1\underline{r}_1, \lambda_2\underline{r}_2, \ldots, \lambda_{n-1}\underline{r}_{n-1}] \tag{39}$$

Next, sort the eigenvalues of $\widehat{A}$ in decreasing order and change the sequence of the vectors $\underline{q}_k$ in Q and $\underline{p}_k$ in P correspondingly. Evaluate the residues according to Eq. (35) and update Eq. (37)–(39). Divide the eigenvalues into N_{RGSS} segments. In a manner similar to the method of the residue grouping with the analytical transfer function, the grouped residues and eigenvalues are given as follows:

$$\underline{r}_{g,i} = \sum_{k=k_{g,i-1}+1}^{k_{g,i}} \underline{r}_k, \quad i = 1, \ldots, N_{RGSS} \tag{40}$$

$$\lambda_{g,i} = \frac{\sum_{k=k_{g,i-1}+1}^{k_{g,i}} \lambda_k \underline{r}_{k,n-1}}{\underline{r}_{g,i,n-1}}, \quad i = 1, \ldots, N_{RGSS} \tag{41}$$

The approximate transfer function using the residue grouping with state space (RGSS) approach is given by:

$$\frac{\underline{y}(s)}{j(s)} = \underline{G}_{RGSS} \doteq \underline{Z}_g + \sum_{i=1}^{N_{RGSS}} \frac{s\underline{r}_{g,i}}{s - \lambda_{g,i}} \tag{42}$$

where $\underline{Z}_g$ is the approximation of Z obtained by substituting Eqs. (40), (41) to Eq. (37)–(39). Recall that the dependent variable in Eq. (31) is the difference between the deviation concentration at the node points except for the first point ($\bar{c}_{s,i}$, $i = 2,\ldots,n$) and the deviation concentration at the first node point ($\bar{c}_{s,1}$). The transfer function of the deviation concentration at the first node point obtained from the previous section (section of Finite Volume Method) should be added to the transfer function shown in Eq. (42) to obtain the transfer function for each of the concentration deviations at the node points from 2 to n. Similarly, the transfer function of the surface concentration difference can be obtained by using a three-point backward difference:

$$\frac{\Delta c_{s,R_s}(s)}{j(s)} = \frac{9}{8}G_{RGSS,n-1}(s) - \frac{1}{8}G_{RGSS,n-2}(s) - \frac{3h}{8D_s a_s F} + \frac{3}{R_s a_s F s} + G_1(s) \tag{43}$$

The frequency response of the surface concentration difference obtained by using the various models shown above can be calculated by replacing Laplace s by $i\omega$ where i is the imaginary unit and ω denotes the frequency in rad s^{-1} Fig. 2 shows a comparison of the magnitudes of the frequency response between the analytical solution and the simplified models. There are an infinite number of negative poles, which are the roots of the eigen-equation: $\tan h(R_s s/D_s) = R_s s/D_s$ in the analytical transfer function of the surface concentration deviation shown in Eq. (10). The solid line shown in Fig. 2 denotes the analytical solution of the frequency response. The dashed line shown in Fig. 2 denotes the results of the truncated analytical solution with the first 50 slowest (smallest in magnitude) poles. For the long time scale (small values of ω) the magnitude of the analytical frequency response approaches to a stable value as expected. As the frequency increases, the logarithm of magnitude of the analytical frequency response goes to a very small value. The boxes represent the frequency response of the 9 terms grouping of the 50th order truncation of the analytical solution. The frequency response obtained using this residue grouping method with 9 groups for the 50th order truncation agrees well with the analytical solution when the frequency is less than about 10 rad sec^{-1}. Due to the loss of the fast poles, the frequency response of the 50th order truncation of the analytical solution tends to a constant value when the frequency is greater than 10 rad sec^{-1}. The frequency responses of the finite volume method with 30, 50, and 80 control volumes are represented by stars, a dotted line, and crosses, respectively in Fig. 2. The frequency responses of all of these FVM cases overlap the analytical solution when the frequency is less than 1 rad sec^{-1}. As the number of control volumes increases, the accuracy of the frequency response of the FVM in the short time scale (high frequency) improves. But the FVM with 80 control volumes is less accurate than the 50th order truncation of the analytical solution in the short time response ($\omega > 10$ rad sec^{-1}). The circles shown in Fig. 2 denote the frequency response of the residue grouping using the state space approach (RGSS). The state space was obtained by using FVM with 50 CVs. The frequency response of the RGSS is close to that of the FVM with 50 CVs when the frequency is less than 0.01 rad sec^{-1} or the frequency is greater than 3 rad sec^{-1}. In the frequency range [0.01 3] rad sec^{-1}, the frequency response of FVM agrees well with the analytical solution, but the frequency response of the RGSS oscillates around the analytical solution. The frequency responses of the two-term polynomial and the three-term polynomial approximations are denoted by the up triangles and diamonds in Fig. 2, respectively. As shown in Fig. 2, the two-term polynomial approximation only captures the long time steady state response. The three-term polynomial approximation is improved somewhat by adding one pole to the two-term polynomial approximation. The pole is given by $-30D_s/R_s$ [2] which equals to 6.0×10^{-3} s^{-1} based on the parameters shown in Table 1. This pole is between the first and the second analytical poles which were obtained by solving the eigen-equation.

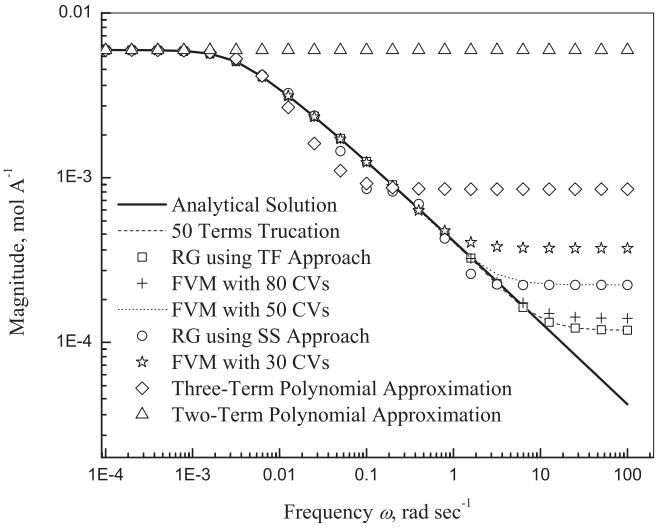

Fig. 2. Frequency response of the simplified models compared to the analytical solution.

3. Orthogonal collocation on finite elements

To use the orthogonal collocation on finite elements technique, the geometry (radial direction in the solid particle) is divided into

Table 1
Parameters for solid phase diffusion [6].

Parameter	Value
Diffusion Coefficient D_s, m^2 s^{-1}	2.0×10^{-16}
Radius of the Particle R_s, m	1.0×10^{-6}
Specific Area a_s, m^2 m^{-3}	1.74×10^6
Faraday's Constant F, C mol^{-1}	96,487
C Rate Current, A	0.272
Total Active Area S, m^2	1.18

number of elements shown in Fig. 3. In each element, the collocation points (i.e., the inner points in an element) are located at the roots of the Jacobi polynomial whose order equals to the number of collocation points in the element. The N^{th} order Jacobi polynomial is defined by [10]:

$$(1-x)^{\alpha}x^{\beta}P_N^{(\alpha,\beta)} = \frac{(-1)^N\Gamma(\beta+1)}{\Gamma(N+\beta+1)}\frac{d^N}{dx^N}\left[(1-x)^{N+\alpha}x^{N+\beta}\right],\quad x\in[0,1] \tag{44}$$

where α and β, coefficients of Jacobi polynomial, determine the locations of the collocation points. When the value of α is increased, the locations of the inner points in each element move closer to the left boundary of the element (r_0^e in Fig. 3). When the value of β is increased, the locations of the inner points move closer to the right boundary of the element (r_1^e in Fig. 3). When both α and β equal zero, the inner node points are symmetric about the center of the element as shown in Fig. 3. Each element is rescaled such that the local coordinate in the element ranges from 0 to 1. As shown in Fig. 3, the element "e" with the size of h_e starts at r_0^e and ends at r_1^e. The relationship between the local coordinate ξ and the global coordinate r is given by:

$$\xi = \frac{r-r_0^e}{h_e} \tag{45}$$

The concentration at the node points in the element e is denoted by $c_{s,j}^e$ where $j = 1,\ldots,N_{OC}+2$, and N_{OC} is the number of inner points. If the same number of inner node points are assigned to all the elements, the total number of node points in the whole geometry is: $N_T = N_E \times (N_{OC}+1)+1$, where N_E denotes the total number of elements. Globally, the concentration at the node points is denoted by C_i where $i = 1,..,N_T$. For element e with $N_{OC} = 4$, the first derivative and the second derivative of the local concentration with respect to the local coordinate can be approximated by: [10]:

$$\frac{d\underline{c}_s^e}{d\xi} = A_{OC}\underline{c}_s^e \tag{46}$$

$$\frac{d^2\underline{c}_s^e}{d\xi^2} = B_{OC}\underline{c}_s^e \tag{47}$$

where $\underline{c}_s^e = [c_{s,1}^e, c_{s,2}^e, c_{s,3}^e, c_{s,4}^e, c_{s,5}^e, c_{s,6}^e]^T$, $c_{s,1}^e$ and $c_{s,6}^e$ represent the concentrations at r_0^e and r_1^e, respectively. Converting the derivatives for the concentration from the local coordinate to the global coordinate according to the relationship between the local coordinate to the global coordinate shown in Eq. (45), we have:

$$\frac{d\underline{c}_s^e}{dr} = \frac{1}{h_e}A_{OC}\underline{c}_s^e \tag{48}$$

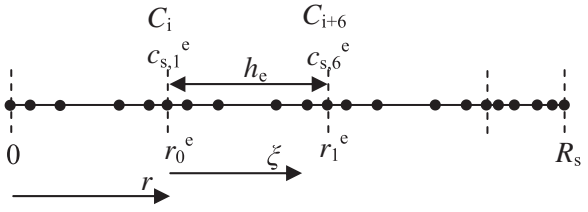

Fig. 3. Schematic of the node points assignment for the diffusion problem using the method of orthogonal collocation on finite elements (number of elements: $N_E = 4$; number of inner points: $N_{OC} = 4$; $\alpha = 0$ and $\beta = 0$).

$$\frac{d^2\underline{c}_s^e}{dr^2} = \frac{1}{h_e^2}B_{OC}\underline{c}_s^e \tag{49}$$

The locations of the node points can be determined by:

$$r_{(e-1)(N_{OC}+1)+j} = r_0^e + h_e R_{OC,j} \tag{50}$$

where $e = 1,\ldots,N_E$, $j = 2,\ldots,N_{OC}+2$, $r_1 = 0$, R_{OC} is a vector of the locations of the roots of N_{OC}^{th} order Jacobi polynomial including the two boundaries of the element. The $N_{OC}+2$ by $N_{OC}+2$ matrices A_{OC}, B_{OC} and the $N_{OC}+2$ by 1 vector R_{OC} can be determined by invoking the routines in Ref. [10] (i.e., JCOBI presented in Appendix A1 in Ref. [10]). The model equations at the inner points (collocation points) in each element were obtained by substituting Eq. (48)–(50) to Eqs. (5)–(7). In the interfaces between the two elements, the mass flux is continuous. The summary of the model equations using the orthogonal collocation on finite elements is given as follows.

At the ith collocation point for element e:

$$\frac{dc_{s,i}^e}{dt} = D_s B_{OC}(i,:)\cdot\underline{c}_s^e + \frac{2D_s}{r_{(e-1)(N_{OC}+1)+i}}A_{OC}(i,:)\cdot\underline{c}_s^e,\quad i = 2,\ldots,N_{OC}+1 \tag{51}$$

where $A_{OC}(i,:)$ is a row vector, and i denotes the ith row in matrix A_{OC}, $\underline{c}_s^e$ is the $N_{OC}+2$ by 1 column vector for the local concentration and the dot between two vectors denotes the dot product.

At $r = r_1^e$ for any element beside of the element N_E:

$$-\frac{D_s}{h_e}A_{OC}(N_{OC}+2,:)\cdot\underline{c}_s^e = -\frac{D_s}{h_{e+1}}A_{OC}(1,:)\cdot\underline{c}_s^{e+1} \tag{52}$$

At $r = 0$ ($r = r0^e$ and $e = 1$):

$$-\frac{D_s}{h_1}A_{OC}(1,:)\cdot\underline{c}_s^1 = 0 \tag{53}$$

At $r = Rs$ ($r = r1^e$ and $e = NE$):

$$-\frac{D_s}{h_{N_E}}A_{OC}(N_{OC}+2,:)\cdot\underline{c}_s^{N_E} = \frac{j(t)}{a_s F} \tag{54}$$

The discrete model using OCFE shown in Eq. (51)–(54) for the 1-D diffusion problem can be rewritten as:

$$M\dot{\underline{C}} = A\underline{C} + \underline{b}j(t) \tag{55}$$

where the mass matrix M is a modified identity matrix in which the diagonal element is 1 for the collocation points and is zero on the interfaces between the elements. The coefficient matrix A in Eq. (55) is a banded matrix with the bandwidth of $2(N_{OC}+1)+1$. The Laplace transform of Eq. (55) is given by:

$$\underline{G}_{OCFE}(s) = \frac{\underline{C}(s)}{j(s)} = (sM+A)^{-1}\underline{b} \tag{56}$$

The transfer function of the difference between the surface concentration and the average concentration using the OCFE method is given by:

$$\frac{\Delta c_{s,R_s}(s)}{j(s)} = G_{OCFE,N_T}(s) + \frac{3}{R_s a_s F s} \tag{57}$$

The frequency response of $\Delta c_{s,R_s}$ using OCFE can be obtained by substituting $i\omega$ for s. Fig. 4 shows the frequency response of $\Delta c_{s,Rs}$ using OCFE with uniform elements, a different number of elements, and a different number of inner points. For the first set of cases, the coefficients α and β used in the OCFE were set to zero. The solutions of OCFE were compared to the solution of FVM with 30 control volumes and the analytical solution. The numbers in the

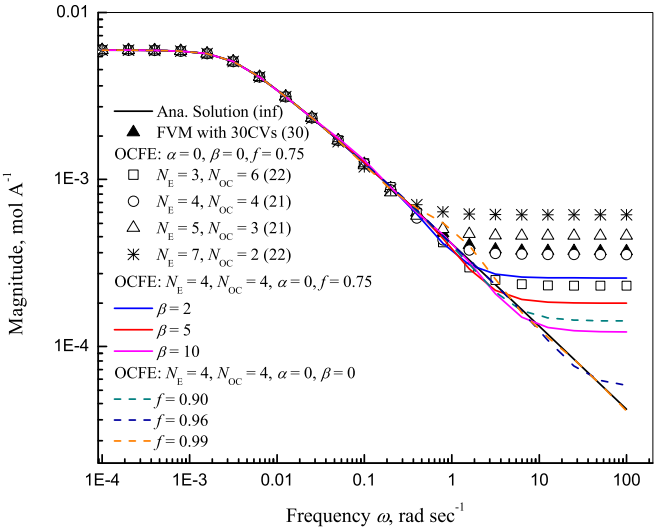

Fig. 4. Effects of the number of elements, the number of collocation points, the value of β, and the size of the element near the particle surface on the frequency response of the surface concentration using OCFE.

parenthesis shown after the model names in Fig. 4 indicate the number of equations in the corresponding discrete models. With a similar number of equations, the discrete model using OCFE with more inner points possesses higher accuracy in the frequency response of $\Delta c_{s,Rs}$. When the number of inner points is equal to 4, the OCFE model with 21 equations (circles in Fig. 4) is more accurate than the FVM with 30 equations (filled triangles in Fig. 4) in the short time response ($\omega = 1$ rad sec^{-1}) of the surface concentration relative to the average concentration.

Fig. 4 also shows the effect of the value of β on the accuracy of the short time response of the surface concentration. Four equal sized elements were assigned to the geometry. In each element, four collocation points were applied and the value of α was fixed to zero. The frequency responses using the OCFE with four different values for β: 0, 2, 5, and 10 were compared to the analytical solution. As the value of β increases, the short time response of the surface concentration relative to the average concentration gets closer to the analytical solution. This is because the higher the value of β is, the closer the collocation points are to the right boundary of the element. For the element near the particle surface, high value of β leads to the locations of the collocation points moving to the surface of the particle, which improves the accuracy of the approximation of the gradient at the surface shown in Eq. (54). Smith and Wang [11]indicated that placing a smaller element near the particle surface helps to achieve a better approximation to the surface concentration. In this work, we used unequal sized elements for the geometry to obtain more accurate short time (large ω values) response of the surface concentration relative to the average concentration. To do this, we defined a factor, f, such that the size of the element near the surface is determined by:

$$h_{N_E} = (1-f)R_s \tag{58}$$

The size of each of the other elements is identical and is determined by:

$$h_e = \frac{fR_s}{N_E - 1}, \quad e = 1, \ldots, N_E - 1 \tag{59}$$

Fig. 4 shows the effects of the factor f on the frequency response of the surface concentration relative to the average concentration. The values of the coefficients α and β were set to zero. The geometry was partitioned into four elements, each of which includes four collocation points. The frequency responses using the OCFE with different values of f were compared to the analytical solution in Fig. 4. The factor f is equal to 0.75 for the case using uniform elements with $N_E = 4$. When f is increased the size of the element near the surface decreases, and the accuracy of the short time response of the surface concentration relative to the average concentration increases. When f is equal to or greater than 0.96, the accuracy of the short time response of the surface concentration relative to the average concentration is improved significantly. Fig. 4 also shows that when $f = 0.99$ the response of the surface concentration relative to the average concentration is much more accurate than that when $f = 0.96$ for ω>=5 rad sec^{-1}. But the response of the surface concentration relative to the average concentration is worse in the frequency region around 1 rad sec^{-1} when $f = 0.99$ compared to the case with $f = 0.96$. This can be corrected by increasing the number of elements or increasing the number of inner points in each element.

The method of OCFE was applied to solve the P2D model for a lithium ion cell with mesocarbon microbead (MCMB) as the anode active material and lithium cobalt oxide as the cathode active material, and 1M $LiPF_6$ in propylene carbonate/ethylene carbonate/dimethyl carbonate mixture as the electrolyte. The parameters for the P2D model which were presented in our previous work [3] and are summarized in Table 2. The open circuit potentials of the active material in the electrodes were given in Ref. [14]. The expressions of the diffusion coefficient of lithium ions in the electrolyte and the ionic conductivity of the electrolyte were presented in Ref. [15]. The particles in the electrodes were divided into four elements in each of which four collocation points were assigned with $\alpha = 0$ and $\beta = 0$. The factor f was set to 0.96 for the discretization of the radius of the particle. The positive electrode and the negative electrode were partitioned into five equal sized elements. And one element was assigned to the separator. In each element in the both electrodes and the separator, five collocation points were assigned with $\alpha = 0$ and $\beta = 0$. The resulting discrete

Table 2
Parameters for the P2D model.

Parameter	Anode (Li_xC_6)	Cathode (Li_yCoO_2)
Thickness, μm	73.5	70.0
Particle radius, μm	12.5	8.5
Solid phase diffusion coefficient, m^2 s^{-1}	5.5 × 10^{-14}[a]	1.0 × 10^{-11}[a]
Reaction rate constant, mol$^{0.5}$ m$^{2.5}$ s^{-1}	1.764 × 10^{-11}[b]	6.667 × 10^{-11}[b]
Maximum concentration in solid phase, mol m^{-3}	30556[c]	51555[c]
Porosity	0.4382[b]	0.3[b]
Volume fraction of fillers	0.0566[b]	0.15[b]
Electronic conductivity, S m^{-1}	100[a]	10[a]
Charge transfer coefficient	0.5[a]	0.5[a]
Bruggeman's number	4.1[b]	1.5[b]
Initial state of charge	0.756	0.465
Temperature, °C	25	
Thickness of separator, μm	25[b]	
Porosity of separator	0.45[b]	
Bruggeman's number in separator	2.3[b]	
Cationic transference number	0.435[b]	
Initial concentration of the electrolyte, mol m^{-3}	1000	
C rate current density, A cm^{-2}	25	

[a] Obtained from Ref. 12.
[b] Obtained from Ref. 13.
[c] Obtained from Ref. 14.

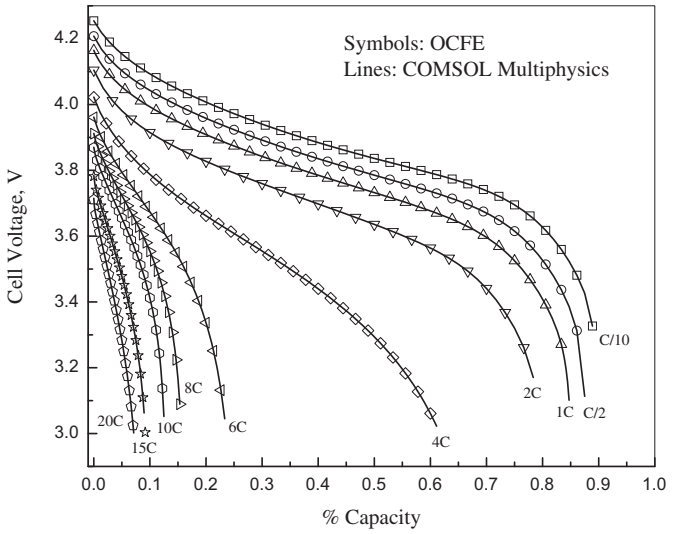

Fig. 5. Comparison of the cell voltage between the P2D model using OCFE and the P2D model solved in COMSOL Multiphysics® for the discharge processes under different current rates varying from C/10 to 20C (lines denote the results from COMSOL Multiphysics and symbols are the results obtained by using the OCFE method).

model using OCFE involving 1608 equations were solved using the DAE solver DASRT under different C rates ranging from C/10 to 20C. The P2D model was also solved in COMSOL Multiphysics® [16], a commercial finite element solver, with the degrees of freedom of 11,270 (number of unknown variables to be solved) and under the same conditions as in the OCFE model. The discharge profiles for both models under the selected C rates are shown in Fig. 5. The symbols denote the results of the OCFE model and the lines denote the results of COMSOL Multiphysics® model. The two models agree well in the current rate range: C/10-20C. And the OCFE model is about 30 times faster than the COSMOL Multiphysics model (approximately 2 s vs. 60 s computation time).

4. Conclusions

In this paper, the methods, which include the polynomial approximation, the residue grouping, and the finite volume method, to solve the 1-D diffusion problem for the frequency response of the surface concentration of the particle were compared to the analytical solution for spherical diffusion with flux boundary conditions. According to the comparisons of the frequency response of the surface concentration relative to the average concentration, it was found that the two-term polynomial approximation only captures the steady state of system and the three-term polynomial approximation provided more accuracy by adding one pole to the transfer function of the surface concentration. The residue grouping with the analytical transfer function approach agrees well with the high order truncation of the analytical transfer function. The accuracy of the residue grouping with the state space approach depends on the accuracy of the original finite volume method upon which the state space model was developed.

The OCFE method was introduced in this paper to solve the diffusion problem in the solid particle. It was found that when the total number of node points is fixed, increasing the number of collocation points by decreasing the number of elements improves the accuracy of the approximation of the surface concentration in the short time scale. It was also found that reducing the size of the element near the surface of the particle significantly improves the accuracy of the approximation of the surface concentration in the short time period. The OCFE method was also successfully applied to solve the P2D model for a lithium ion cell and reduced the computation time by approximately 30 times compared to COMSOL Multiphysics®.

Acknowledgment

The authors gratefully acknowledge the funding support provided by QUALLION LLC under the MDA project STTR Phase II (contract no. HQ0006-09-C-7074): Rechargeable Lithium Ion Battery Operating Life Model.

List of symbols

a_s	pecific area of the electrode, $m^2\ m^{-3}$
A	coefficient matrix
A_{OC}	matrix in the approximation of the first order derivative using OCFE method
$\underline{b}$	source term vector
B_{OC}	matrix in the approximation of the second order derivative using OCFE method
c_s	concentration of lithium ions in solid phase, mol m^{-3}
$\underline{C}$	vector of concentration at the node points, mol m^{-3}
D_s	diffusion coefficient of lithium ions in solid phase, $m^2\ s^{-1}$
F	Faraday's constant, 96,487 C mol^{-1}
G	transfer function vector
h	size of the control volume
h_e	size of the element e
I	identity matrix
I_{app}	applied current, A
$j(t)$	time dependent volumetric current density, A m^{-3}
M	mass matrix
N_E	number of elements
N_{OC}	number of collocation points
N_T	total number of node points
p	pole of the transfer function
R_{OC}	vector of the positions of the collocation points
R_s	radius of the particle, m
s	independent in Laplace domain
Z	steady state of the transfer function

Greek

α	coefficient of Jacobi polynomial
β	coefficient of Jacobi polynomial
ξ	local coordinate in radial direction in the particle
ω	frequency, rad s^{-1}

Subscript

avg	average
R_s	evaluated at the surface of the particle
max	maximum

Superscript

-1	matrix inverse
e	element index
T	matrix transpose

References

[1] M. Doyle, T.F. Fuller, J. Newman, J. Electrochem. Soc. 140 (1993) 1526.
[2] T.F. Fuller, M. Doyle, J. Newman, J. Electrochem. Soc. 141 (1994) 1.
[3] L. Cai, R.E. White, J. Electrochem. Soc. 156 (2009) A154.
[4] L. Cai, R.E. White, J. Electrochem. Soc. 157 (2010) A1188.
[5] V.R. Subramanian, V.D. Diwakar, D. Tapriyal, J. Electrochem. Soc. 152 (2005) A2002.

[6] K.A. Smith, C.D. Rahn, C.Y. Wang, J. Dynamic Systems, Measurement, Control 130 (2008) 011012–011021.
[7] C.Y. Wang, W.B. Gu, B.Y. Liaw, J. Electrochem. Soc. 145 (1998) 3407.
[8] V. Ramadesigan, V. Boovaragavan, J.C. Pirkle Jr., V.R. Subramanian, J. Electrochem. Soc. 157 (2010) A854.
[9] T. Jacobsen, K. West, Electrochim. Acta 40 (1995) 255.
[10] J. Villadsen, M.L. Michelsen, Solution of Differential Equation Models by Polynomial Approximation, Prentice-Hall, Inc., Englewood Cliffs, N.J, 1978, p. 417.
[11] K. Smith, C.Y. Wang, J. Power Sources 161 (2006) 628.
[12] M. Doyle, R. Fuentes, J. Electrochem. Soc. 150 (2003) A706.
[13] K. Kumaresan, G. Sikha, R.E. White, J. Electrochem. Soc. 155 (2008) A164.
[14] P. Ramadass, B. Haran, P.M. Gomadam, R.E. White, B.N. Popov, J. Electrochem. Soc. 151 (2004) A196.
[15] L.O. Valoen, J.N. Reimers, J. Electhochem. Soc. 152 (2005) A882.
[16] COMSOL Multiphysics ®, online: http://www.comsol.com/, accessed Mar. 20, 2012.